Application of intravital microscopy in studies of tumor microcirculation

Sarah Jane Lunt
University of Sheffield
School of Medicine
Tumour Microcirculation Group
and
Department of Oncology
Beech Hill Road
Sheffield, S10 2RX
United Kingdom

Colin Gray
University of Sheffield
School of Medicine
Department of Cardiovascular Science
Beech Hill Road
Sheffield, S10 2RX
United Kingdom

Constantino Carlos Reyes-Aldasoro
University of Sheffield
School of Medicine
Tumour Microcirculation Group
and
Department of Oncology
Beech Hill Road
Sheffield, S10 2RX
United Kingdom

Stephen J. Matcher
University of Sheffield
The Kroto Institute
Broad Lane
Sheffield, S3 7HQ
United Kingdom

Gillian M. Tozer
University of Sheffield
School of Medicine
Tumour Microcirculation Group
and
Department of Oncology
Beech Hill Road
Sheffield, S10 2RX
United Kingdom

Abstract. To grow and progress, solid tumors develop a vascular network through co-option and angiogenesis that is characterized by multiple structural and functional abnormalities, which negatively influence therapeutic outcome through direct and indirect mechanisms. As such, the morphology and function of tumor blood vessels, plus their response to different treatments, are a vital and active area of biological research. Intravital microscopy (IVM) has played a key role in studies of tumor angiogenesis, and ongoing developments in molecular probes, imaging techniques, and postimage analysis methods have ensured its continued and widespread use. In this review we discuss some of the primary advantages and disadvantages of IVM approaches and describe recent technological advances in optical microscopy (e.g., confocal microscopy, multiphoton microscopy, hyperspectral imaging, and optical coherence tomography) with examples of their application to studies of tumor angiogenesis. [DOI: 10.1117/1.3281674]

Keywords: intravital microscopy; optical imaging; window chamber; tumor microcirculation; angiogenesis; vascular targeting.

Paper 09405SSR received Sep. 11, 2009; revised manuscript received Oct. 20, 2009; accepted for publication Oct. 22, 2009; published online Feb. 9, 2010.

1 Biological Significance of Tumor Microcirculation

It is a well-established concept that the continued growth and progression of a tumor is dependent on the development of a vascular network to supply oxygen and nutrients.[1] Tumors develop a vascular network through co-option of the surrounding normal vasculature and/or angiogenesis—the development of neovasculature from preexisting vessels.[2,3] The blood vessels formed by these processes are characterized by multiple structural and functional abnormalities, including tortuous vascular networks, neovascular shunts, blind ends, plasma channels, and temporally as well as spatially heterogeneous blood flow.[4–9] These abnormalities result in tumor regions with poor delivery of oxygen and nutrients, resulting in hypoxia and low pH, as well as high vascular permeability and microvessel resistance, which contribute to elevated tumor interstitial fluid pressure (IFP).[10,11] Tumor hypoxia, acid-

Address all correspondence to: Gillian M. Tozer, University of Sheffield, Department of Oncology, K Floor, School of Medicine, Beech Hill Road, Sheffield S10 2RX, UK. Tel: 44(0)114 271 2423; Fax: 44(0)114 271 3314; E-mail: g.tozer@sheffield.ac.uk.

1083-3668/2010/15(1)/011113/14/$25.00 © 2010 SPIE

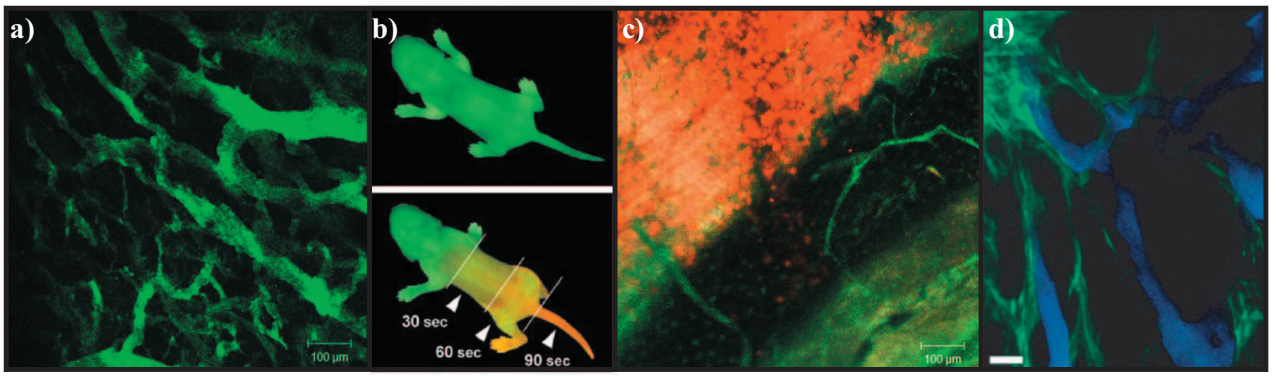

Fig. 1 Fluorescent probes. (a) Multiphoton image of FITC-dextran labeled blood vessels in a murine fibrosarcoma growing in the dorsal skin fold window chamber (DSFC). (b) A neonatal Kaede transgenic mouse (reprinted with kind permission from Tomura et al.[141]) before (upper) and after (lower) photoconversion on exposure to ultraviolet light for 30, 60, or 90 sec. (c) Fluorescent image of human prostate carcinoma (PC3) tumor constitutively expressing mCherry growing in the DSFC of a transgenic Tie2-GFP mouse. Tumor cells are red, and GFP expression is visible in the blood vessel walls. (d) Multiphoton image depicting the use of quantum dots (reprinted with kind permission from Stroh et al.[42]) in vascular imaging of a MCaIV mammary tumor growing in the DSFC of a VEGF-GFP transgenic mouse. The figure shows concurrent imaging of quantum dot labeled blood vessels (QD470, blue) and VEGF-driven GFP expression in perivascular cells. Concurrent imaging at 850 nm was possible due to the broad excitation spectrum of the quantum dots (scale bar, 50 μm).

ity, and IFP have been related to disease progression and adverse therapeutic outcome.[12,13] In addition to the clinical impact of these indirect features of tumor vascular abnormalities, tumor vessel density has been directly related to a poor prognosis in multiple studies.[14–17] The key requirement for tumor angiogenesis in tumor progression, coupled with its clinical significance, highlight the tumor vasculature as a potential biomarker of disease status and exploitable therapeutic target. Thus, to take full advantage of the tumor vasculature as a target, it is necessary to understand the processes involved in tumor vascularization, the structural and functional abnormalities that characterize tumor vessels, and their response to therapy. A large part of what is known to date from *in vivo* studies has been uncovered using optical imaging, more specifically intravital microscopy (IVM). We discuss some of the different IVM approaches—what has been shown to date, and current and future applications of optical imaging in tumor angiogenesis.

2 Optical Imaging and Intravital Microscopy

Optical imaging describes the use of the visible spectrum extended to include ultraviolet and near infrared (~300 to 1300 nm) light imaging. Macroscopic bioluminescence and fluorescence techniques are becoming commonplace in cancer research for *in vivo* studies of the tumor microenvironment, particularly induction of and changes in hypoxia and tumor cell metastasis/invasion.[18–20] However, microscopic optical imaging of tumors *in vivo* (intravital microscopy or IVM) enables high resolution studies at a cellular/subcellular level in real time, with applications in clinical as well as experimental animal research, via technological advances such as microendoscopy.[21,22] Recent advances in fluorescent/bioluminescent probes, microscopes and associated filters, image acquisition, and analysis technology have ensured continued development of IVM as a valuable research tool in the field of tumor angiogenesis and microcirculation, permitting the study of tumor cell interactions with stroma/blood vessels,[23,24] gene expression and vascular function[25,26] – blood supply[27,28] and vascular permeability,[29,30] among others.

3 Fluorescent Probes for Bioimaging

Many different types of probes are available for optical imaging and IVM[31,32] from fluorescent dyes[33–35] to photoactivatable and photoswitchable fluorescent proteins[32,36,37] (see Fig. 1).

Fluorescein isothyocyanate (FITC) is an organic fluorescent dye that continues to be widely used after several decades.[33,38] It has excitation and emission maxima at 488 and 520 nm, respectively, and demonstrates high fluorescence intensity, but like many fluorophores, particularly organic ones, is prone to photobleaching. This has led to the development of synthetic dyes such as the Alexa-fluor dyes (Alexa-fluor 350, 488, 555, etc.) that demonstrate improved photostability alongside high intensity. FITC can be conjugated to different molecules. For instance, dextrans are polysaccharides composed of glucose chains of varying lengths; consequently, multiple molecular weight versions of FITC-dextran exist, and can be used to provide valuable information on vascular permeability through analysis of vascular leak.[38]

In addition, there are chemically sensitive derivatives of FITC, such as the pH sensitive fluorochrome 2′, 7′-bis-(2-carboxyethyl)-5,6-carboxyfluorescein (BCECF). BCECF excitation occurs in a pH-dependent manner at wavelengths between 440 and 500 nm, and has been used to generate spatial and qualitative data on tumor pH.[39] The fluorescence spectra of porphyrins are also pH sensitive, and phosphorescence lifetime is oxygen sensitive, enabling elegant studies of the tumor microenvironment.[40]

Although useful, organic dyes have several limitations. In addition to photobleaching, they generally exhibit broad emission spectra, which limit their capacity as dual markers of different events/structures because of cross talk between the dyes. Quantum dots represent a class of fluorescent nanocrystals synthesized to have broad excitation peaks and sharp

emission peaks to overcome these limitations.[35,41] They exist in a range of colors, and generate bright fluorescence with improved photostability, making them less prone to photobleaching, an important and desirable property for live imaging studies that might involve prolonged and repeated exposure times. Stroh et al.[42] exploited the broad excitation peak of quantum dots to image MCaIV murine mammary tumor vasculature (following IV injection of quantum dots) and perivascular cells simultaneously [VEGF-GFP transgenic mice expressing VEGF-driven green fluorescent protein (GFP)] using the same wavelength [see Fig. 1(d)].

In recent years, fluorescent probes have been developed to exploit a process known as Förster resonance energy transfer (FRET). If two different fluorophores are located within the Förster radius (typically 10 nm) of each other and one has a peak emission wavelength that is broadly the same as the peak excitation wavelength of the other (i.e., significant emission-excitation spectral overlap), a nonradiating energy transfer can occur (FRET). The emission energy will transfer from the first fluorophore to the second non-radiatively. For example, on exposure to indigo/blue light, a cyan fluorescent protein (CFP) molecule (the donor) in close proximity to a yellow fluorescent protein (YFP) molecule (the acceptor) will cause the YFP to emit yellow light without having been exposed to the green light normally required to excite its fluorescence. This technique is used to demonstrate molecular interaction and colocalization, and has been used primarily for studies of cells *in vitro*. However, Zhou et al.[43] recently described *in vivo* use of a FRET probe molecule consisting of eCFP linked to Venus (a yellow fluorescent protein variant, see discussion later on), with a sequence containing a caspase-3 cleavage site. They used this probe to monitor the dynamics of caspase-3 activation induced by the action of the drug cisplatin and photodynamic therapy in tumors using FRET IVM. On caspase-3 activation, the molecular link between the eCFP and Venus is broken and the FRET signal is lost. Similar FRET probes have been used, in mouse tumor models *in vivo*, to investigate the activity and therapeutic targeting of matrix metalloproteinases, enzymes intimately involved in angiogenesis.[44]

The discovery of green fluorescent protein (GFP) in 1962,[45,46] and the plethora of fluorescent proteins that have been uncovered, refined, and synthesized since, has revolutionized *in vivo* optical imaging. The literature available on the use of GFP and other fluorescent proteins (BFP, CFP, YFP, RFP)[32] is vast. The main use of these proteins is to fuse them to genes of interest that in turn regulate their expression, so that fluorescence is used as a reporter of gene expression *in vivo*, at multiple time points. IVM studies of tumors using GFP and similar proteins have primarily focused on tumor cells transfected with the corresponding gene, under the control of a constitutively expressed viral promoter. This allows microscopic tracking of tumor cell proliferation and migration patterns.[47] Fluorescence of GFP does not require specific cofactors but does depend on oxygen concentration,[48] such that data need to be interpreted with caution. The potential for such large proteins to modify cell behavior is also a concern, although several studies have demonstrated minimal effects of GFP in tumor cells on such properties as tumor progression and metastasis.[49] Several fruit fluorescent proteins have been developed more recently, which are mutants of a monomeric mutant form of dsRed (mRFP1). These proteins (e.g., mCherry and TdTomato) are potentially less disruptive than GFP, and also provide a range of colors from yellow-orange to red-orange, with improved quantum efficiency and stability.[50] To date these proteins have not been used in IVM studies of tumors; however, their suitability for *in vitro* live cell imaging studies has recently been explored,[51] and it is likely that newer gene expression vectors will be synthesized to exploit their advantages.

Proteins demonstrating reversible and irreversible changes to their spectral properties on exposure to specific optical wavelengths have now been discovered and developed through modification and refinement of existing fluorescent proteins. These are referred to as photoactivatable (photoactivated shift from low to high fluorescent intensity) or photoswitchable (photoactivated shift in fluorescent color) fluorescent proteins (PAFP).[37,52]

The first natural PAFP to be discovered was Kaede in 2002,[53] which initially fluoresces green, but on exposure to UV light undergoes an irreversible conversion to a red-fluorescent form. In the same year, a photoactivatable mutant version of GFP was synthesized, PA-GFP, exhibiting a wavelength-specific conversion to an enhanced fluorescent form.[52,54] Dronpa and KFP1 exemplify reversible PAFPs.[55,56] Dronpa, which fluoresces green, has the capacity for reversible wavelength-specific bleaching,[55] whereas KFP1 exhibits both reversible and irreversible changes in fluorescent expression—exposure to specific wavelengths can be used to induce relatively short-lived bright red fluorescence that can be quenched, or the exposure times or intensity can be increased to stimulate irreversible "kindling" of red fluorescence that cannot be quenched and does not fade.[56] Although the potential of these proteins has yet to be fully explored, they represent novel and highly useful tools. For example, the idea of inducing an irreversible photoconversion in a cell population of interest and then tracking that population, relative to new incoming cells that have not undergone photoconversion, is an attractive one. Care needs to be taken because new cells produced on cell division will express the fluorescent protein in its original form (e.g., Kaede), thus diluting the population of interest. Nonetheless, with careful planning there is a wide scope for use of these proteins.

4 Dorsal Skin Fold Window Chamber

The dorsal skin fold window chamber model (DSFC) (see Fig. 2) is an invaluable tool for IVM of tumor angiogenesis.[57] It was originally developed in the rabbit ear in 1924[58] and adapted for use in mice in 1943.[59] The DSFC model in mouse involves the surgical removal of a skin flap and associated connective tissue and fat from the dorsum to provide optical clarity. A metal chamber (usually aluminium or titanium) holds the skin away from the mouse body, exposing the vascularized layer of muscle and skin on the opposing side of the flap or "window." A tumor piece or tumor cells (often as a spheroid or cell conglomerate) are placed onto, or injected into, the exposed fascial plane and covered with a glass coverslip. This process is described in detail by Koehl, Gaumann, and Geissler.[57] It should be noted that for larger animals (e.g., rat) that have thicker skin, the skin layers from both opposing

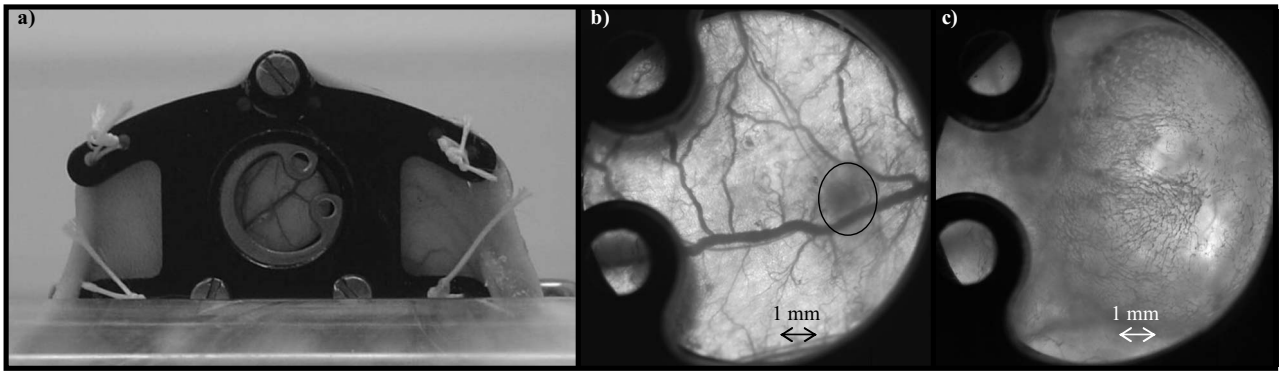

Fig. 2 Dorsal skin fold window chamber (DSFC). (a) A photograph is shown of a DSFC preparation on the rear dorsum of a SCID mouse. The exposed blood vessels on the fascial surface can be clearly seen. (b) A full view of a DSFC window 1-day postimplantation with a tumor cell aggregate (circled; murine fibrosarcoma). (c) The same tumor shown 6 days later, nearly filling the window.

sides of the flap are removed, thereby facilitating an improved optical path.[60]

The DSFC model enables repeated acquisition of spatial and temporal data from a growing tumor over periods of days to weeks. Although there are also several disadvantages (tumors are essentially subcutaneous and there are size restrictions due to the width and diameter of the chamber window, which exert high tissue pressures), the model is widely applicable and has been used extensively in a range of different rodent models, enabling the use of syngeneic rodent tumor lines in immunocompetent strains, as well as human xenograft lines using immunocompromised strains such as nude and severe combined immunodeficiency (SCID) mice.

It should be noted that although the DSFC model is the most extensively used, there are alternative preparations suitable for IVM, the most similar of which is the cranial window, used to expose the brain[34] and mammary window.[61] Other models often require externalization of an organ and thus sacrifice of the animal immediately on completion of image acquisition. Examples include the lung,[62,63] pancreas,[64] mammary fat pad,[65] and mesentery.[66]

5 Intravital Microscope

There are several technical problems to overcome and welfare issues to address when using live animals for microscopy, i.e., positioning and restraint of the mouse, physiological status of the mouse, objective lens properties (sufficient magnification, working distance, and numerical aperture), detector specification, analysis software capabilities, and so on. A standard microscope stage cannot be used, but needs to be specially modified to enable positioning of the mouse such that the window is locked in place. This generally involves the use of a specialized jig that restrains the mouse, with the window in the correct position to be bolted securely to the stage. Further, depending on the time frame of image acquisition, physiological parameters such as body temperature and blood pressure need to be monitored and maintained, necessitating the use of a heating blanket and/or heat lamp and temperature/blood pressure probes and recording equipment for anesthetized animals. Both general anesthesia and physical restraint can confound data interpretation due to alterations in blood pressure and vasoactivity. Isofluorane is commonly considered the most appropriate general anesthetic for small rodents,[67] although constant infusion of a short-lived IV injectable anesthetic such as Propofol can also maintain a suitable anesthetic depth for restraint.

Most IVM studies have to work around movement in the specimen during data acquisition due to pulse, respiration, peristalsis, muscle contraction etc. Without doubt the simplest and most widely used solution to this problem is real-time (video rate) data acquisition with a digital video (DV) camera and images recorded onto tape or other storage media. The major drawback with this approach is that DV cameras do not normally have sufficient sensitivity for use with many fluorescence applications although they are well-suited to transmitted light microscopy. Wide-field fluorescence and Nipkow disk-based confocal microscopes are normally used with cooled charge-coupled device (CCD) cameras, which are more sensitive. Recent further development of these has seen the introduction of back-illuminated (also called back-thinned) CCD cameras that have much higher quantum efficiency and wider spectral response. When coupled to electron multiplication (EM) technology, these detectors (EMCCD) can achieve ~90% quantum efficiency coupled with short-noise-limited at video rate (25 to 30 frames/s).[68] Point scanning laser confocal and multiphoton microscopes usually have photomultiplier tube (PMT) detectors. Although these microscopes are generally slow scanning and the detectors have lower quantum efficiencies than cooled CCDs, nonetheless these systems produce higher resolution images with better contrast than wide-field systems provided that the specimen can be kept still. Multiphoton microscopes do not require pinholes, so can benefit from the increased sensitivity of gallium arsenide phosphide (GAsP) detectors in a nondescanned (NDD) configuration. There are several recent reviews on CCD sensors,[69–72] and the books by Sluder and Wolf[73,74] present a good introduction to cameras for microscopy.

6 Conventional Wide-Field Light Microscopy

6.1 *Background*

Early IVM studies were confined to conventional wide-field light microscopy using transillumination (light transmitted from the condenser through the tissue sample to the objective) or epi-illumination (light reflected/emitted by the tissue

sample through the objective). Basic fluorescent microscopy uses mercury or xenon arc lamps in conjunction with specific excitation and emission filters and a dichroic mirror, which splits the emission and excitation beams. Following exposure to light of an appropriate wavelength, a single photon absorbed by a fluorophore, either intrinsic or an extrinsic fluorescent dye/probe, enters an excited state. While excited, some energy is dissipated so when, after a few nanoseconds, the fluorescent molecule returns to its ground state, a photon of lower energy (and therefore longer wavelength) is emitted. The difference between the excitation and emission wavelength maxima is called the Stokes shift.

Conventional microscopy has been the mainstay of IVM, providing morphological information on the tumor vasculature [see Fig. 3(a)] such as vessel length, diameter, and branching patterns, and qualitative information on the leakiness of blood vessels (hemorrhage), as well as video recordings of flowing blood (contrast provided by red cells under transillumination) and of vascular leak of exogenous fluorescent markers (epi-illumination). Some of the earlier observations made using IVM to study tumors growing in chamber models demonstrated notable architectural and blood flow aberrations that are now widely accepted to characterize tumor vasculature,[75,76] e.g., inconsistency in microvessel size, commonly with larger vessels located at the tumor periphery and smaller, more chaotic vessels toward the center. Dilated capillary diameters varying along the length of abnormally long capillaries were recorded, as well as intermittent or regurgitant flow and temporary or permanent microvessel occlusion by red cells.[75,76] These observations have been strengthened by subsequent refinements and application of modern image analysis techniques.[27,38,77–82]

6.2 *Blood Flow and Vascular Permeability*

Spatial and temporal heterogeneity of tumor blood flow are key contributory factors in the development of the pathophysiolgical tumor microenvironment. Measurement of red cell velocity within individual tumor microvessels can be obtained relatively easily in IVM by modern tracking algorithms.[27] However, this measure is not directly related to tumor blood flow rate (volume of blood delivered to the capillary network per unit volume of tissue per minute), which dictates oxygen and nutrient delivery to tissue. To estimate tissue blood flow rate, a common approach is to inject a contrast agent into the blood stream and measure its concentration time course in arterial blood (input function) and in the tissue of interest (tissue response function). Blood flow rate is then estimated from a mathematical model relating the tissue response function to the input function.[83] Radiotracers are often used as contrast agents, where measures of concentration are easily obtainable. However, in optical imaging, where contrast is obtained from fluorescent agents, quantification of fluorescence intensity (to obtain relative measures of concentration) is a nontrivial exercise. This is because measured fluorescence intensity is highly dependent on several factors that contribute to background and noise, in addition to concentration of the fluorophore. These factors arise from the specimen itself, e.g., stability of fluorescence; the microscope, e.g., spherical aberration; or the detector, e.g., low dynamic range.[84] For these reasons, obtaining accurate estimates of tumor blood flow rate by IVM is difficult. Nevertheless, temporal alterations in tumor blood supply have been measured[85] using an elegant first-pass imaging technique first described by Oye et al.[28] This technique is based on the movement of high molecular weight TRITC-dextran (155 KDa) from the

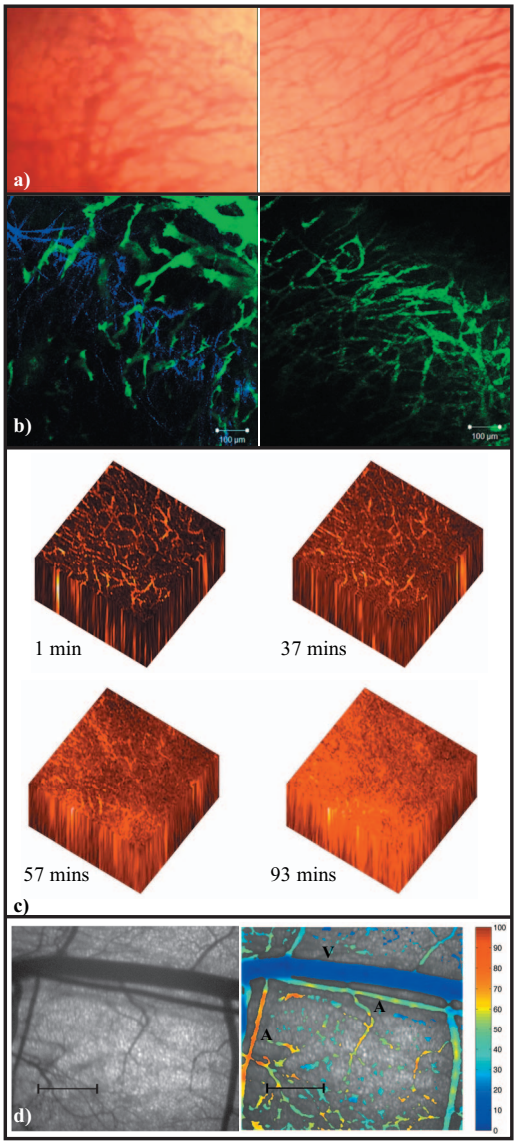

Fig. 3 Images acquired using different microscopy techniques. (a) Transillumination images of murine fibrosarcomas expressing single VEGF isoforms (left is VEGF 120, and right is VEGF 188) growing in the DSFC of SCID mice. Obvious differences in the vascular architecture are apparent. (b) Multiphoton image of murine fibrosarcomas expressing single VEGF isoforms (left is VEGF 120, and right is VEGF 188) following IV administration of FITC-dextran. Second harmonic generation imaging shows collagen fibers (blue) between the vessels (green) in the VEGF 120 tumors. (c) Multiphoton 3-D images of a P22 rat sarcoma growing in the DSFC of BDIX rats following IV administration of FITC-dextran. Four sequential images are shown. The time postinjection is indicated next to each figure, demonstrating vascular leak over time. (d) Transillumination vascular image (left), with adjacent oxyhemaglobin saturation overlay derived from hyperspectral imaging (right) of vasculature in a nontumor-bearing DSFC of a SCID mouse (scale bar, 1 mm). The right-hand axis depicts oxygen saturation from 0 to 100%.

main tumor supplying artery through the tumor vascular network to the main tumor draining vein, visualized using fluorescence IVM to acquire high-frame-rate videos of the fluorescent marker postinjection. A semiquantitative measurement of tumor blood flow was then obtained through examination of fluorescence intensity versus time curves plotted for multiple regions of interest (representing multiple tumor vessels).[28] Repetition of this process over 20-min time intervals within the same tumors demonstrated substantial heterogeneity in blood supply over time in A-07 human melanoma tumors.[85]

Vascular permeability of tumor blood vessels has been widely studied using IVM. This is because the vascular wall represents a barrier to delivery of high molecular weight anticancer agents[86]; an increase in tumor vascular permeability is an early indicator of vascular damage induced by tumor vascular damaging agents[87]; and high vascular permeability is an important characteristic of tumors, with established links to tumor angiogenesis, progression, and poor therapeutic outcome.[12,13,86] The classic methodology for examining tumor microvascular permeability is to analyze the clearance kinetics of a fluorescently labeled molecule (usually BSA or dextran) from the blood vessels to the interstitium following intravenous injection.[34,88,89] The high spatial resolution of IVM allows fluorescence intensity to be measured within and immediately outside individual microvessels, which is an advantage over radiotracer methods for estimating vascular permeability but with the same limitations for quantification of fluorescence intensity, as described before. High molecular weight labeled molecules are chosen to mimic leak of plasma proteins and to provide a relatively low leakage rate, as most calculations of vascular permeability use mathematical models that are based on unidirectional transport across the vascular wall.[29] Elevated tumor vascular permeability has been demonstrated in multiple tumor models using this approach, although methods of analysis have varied.[90–92] Furthermore, more specific features of vascular permeability, such as the inherent variability between different tumor models[34] and increased vascular pore sizes,[88,93] have been shown through similar methods. 3-D imaging of fluorescence, especially using multiphoton fluorescence techniques, has significantly aided quantification of fluorescence intensity. Although they are not currently suitable for tracking fast kinetics (e.g., blood flow), these techniques have been applied to estimation of vascular permeability, as described in Sec. 8.[29]

6.3 *Interstitial Transport*

A fluorophore may go through many excitation-emission cycles, but eventually it will lose the ability to respond. This is a key problem associated with fluorescence microscopy, in that exposure to high intensity light may quite quickly destroy the fluorophore in a process known as photobleaching, particularly problematic if trying to image the same region over time as is often the case when examining tumor vasculature using IVM. Although photobleaching is a complication, it may be exploited through fluorescence recovery after photobleaching (FRAP).[94–96] This technique is particularly useful in studying diffusion or movement of specific molecules through tissue, and involves the application of intense light to bleach a small region of interest, i.e., loss of fluorescent signal within the selected region. The rate of diffusion/active transport of fluorescently labeled molecules into this region can then be measured through increasing levels of fluorescence intensity; for example, Chary and Jain[96] used FRAP to measure tumor (VX2 carcinoma in rabbit ear chamber) interstitial fluid velocity and diffusion following the intravenous administration of FITC conjugated bovine serum albumin (BSA). In addition to providing pertinent information on these parameters in a pathological microenvironment, they were able to observe the direction and velocity of interstitial fluid flow relative to microvascular flow, showing that sudden changes in the direction of RBC flow did impact interstitial flow, although there was a lag in response time.[96]

6.4 *pH and Oxygenation*

Helmlinger et al.[40] used the organic dyes BCECF and porphyrin to examine pH and oxygenation (pO_2) levels of tumor tissue (LS174T, human colon adenocarcinoma) in relation to the tumor vasculature. They found that the majority of the tumor vessels exhibited a higher pH proximally, which decreased moving away from the vessels, although there was little or no pH gradient in some cases. In contrast, pO_2 gradients, which did not correlate with pH, were much more variable, although values were consistently low in avascular areas and at distances greater than 150 μm from the supporting vasculature. However, there are confounding factors in interpreting pO_2 values in tumors growing in the window chamber, as demonstrated in a study using the rat mammary adenocarcinoma (R3230AC) model.[97] As these tumors were grown in DSFCs in rats, both skin layers were removed, permitting imaging of both the fascial and tumor surfaces. Similar to Helmlinger et al.,[40] pO_2 was examined using phosphorescence lifetime imaging of porphyrin. Furthermore, blue and green excitation wavelengths were used due to their differences in tissue penetration (approximately 50 and 200 μm, respectively). This study neatly illustrated a longitudinal gradient in pO_2 values from the fascial through to the tumor surface, a consequence of vascular co-option from the fascial arterioles on tumor implantation.

6.5 *Regulation of Angiogenesis*

Fluorescence IVM studies have broadened our understanding of the onset of angiogenesis and the molecular processes involved in its regulation.[77] Molecular probes have played a key role in these studies, particularly GFP. A seminal study by Li et al.[23] examined the onset of tumor angiogenesis in the DSFC model from a minimal number (20 to 50) of mammary tumor cells (R3230Ac and 4T1). This was possible due to the generation of tumor cells stably expressing GFP, enabling visualization of individual cells using fluorescence microscopy. Tumor growth and angiogenesis were tracked over a 4-week period, showing evidence for early angiogenesis in the form of microvessel dilation and tortuosity within 6 days (60 to 80 tumor cells) of implantation, functional microvessels within 8 days (300 to 400 tumor cells), and an established vascular network by 20 days (4 to 7 mm diameter). Furthermore, tumor cells were found to migrate to, and align themselves alongside, the existing host vasculature in the early stages of angiogenesis, and the vascular network was seen to branch out from the host vasculature in the established tumor. The

same study went on to show that the simultaneous introduction of an antiangiogenic truncated version of the VEGF receptor alongside the tumor cells severely repressed tumor angiogenesis and subsequent tumor growth, thereby providing information on the molecular processes involved in early response and supporting evidence for the importance of angiogenesis in tumor development.[23] Similar studies have examined other proangiogenic proteins and their potential for therapeutic inhibition.[80]

Cao et al.[98] examined the role of hypoxia in tumor angiogenesis using fluorescence IVM. Colon (HCT116) and mammary (4T1) carcinoma cells were engineered to stably express RFP as well as GFP under control of a hypoxia responsive element (HRE), making GFP expression dependent on the presence of hypoxia-inducible factor 1 (HIF-1). When grown in the DSFC, early vessel sprouting was apparent prior to expression of GFP, suggesting that, in this model, the onset of angiogenesis was not dependent on hypoxic conditions. However, the expression of HIF-1 was found to correlate with increased angiogenesis, measured quantitatively through microvessel length/density. Furthermore, microvessels were found to grow toward regions of hypoxia.[98]

6.6 *Response to Therapy*

Both transmitted light and fluorescence microscopy techniques have been widely applied to preclinical studies of vascular targeted therapeutics. Therapeutic approaches using antiangiogenic and vascular disrupting agents (VDAs) have been extensively studied, either as a single agent or in combination regimens, as a result of the direct and indirect impact of tumor vasculature on treatment efficacy. IVM has proved to be a useful tool in examining the vascular effects of these agents. For example, fluorescence microscopy was used to show a reduction in the overall microvessel density of GFP expressing pancreatic adenocarcinoma (Panc-02-HO) and colonic carcinoma (CT-26) tumor models following treatment with the antiangiogenic agent TNP-470.[99] Tozer et al.[38,79] demonstrated that treatment with the VDA combretastatin-A-4-phosphate (CA-4-P) induced a rapid and comprehensive reduction in blood vessel length and density as well as red blood cell velocity using both light and fluorescent IVM approaches. Further, the use of single VEGF isoform expressing murine fibrosarcoma tumors with diverse levels of vascular maturity provided novel data on the impact of vascular maturity on CA-4-P efficacy; the more mature tumor line (VEGF 188 expressing) was found to be significantly less responsive to CA-4-P.[38]

Combination therapy approaches are complicated by how changes wrought by one agent on the tumor vasculature or tumor microenvironment as a whole might influence the efficacy of the second agent. For example, the antivascular effects of vascular targeted therapeutics might be expected to hinder delivery of a secondary drug. However, Czabanaka et al.[100] found that delivery of the chemotherapeutic agent doxorubicin was not impaired when administered sequentially to the multitargeted receptor tyrosine kinase inhibitor sunitinib. Using a human glioma model (SF126), they showed that although sunitinib significantly reduced both total and functional vessel density, the remaining vessels demonstrated improved blood flow. Consequently, the subsequent administration of doxorubicin via the carotid artery resulted in improved interstitial uptake in perivascular regions, and thus a comparable uptake to that seen in tumors that did not receive sunitinib. These data suggest that conventional chemotherapy might be used effectively with vascular targeted therapy. Subsequently, this vascular normalization phenomenon has been demonstrated for other vascular targeted drugs[101] (see Sec. 8 on multiphoton microscopy).

In addition to chemotherapy, vascular targeted therapy is likely to be combined with radiotherapy. One study used conventional light IVM to show that a broad VEGFR tyrosine kinase inhibitor AZD2171 significantly reduced microvessel density in a human lung carcinoma model (Calu-6), and further, that this effect was ameliorated on pretreatment of the tumor with radiation therapy.[102]

7 Confocal Microscopy

Despite the continued utility of conventional wide-field transmitted light and fluorescence microscopy in IVM, there are several problems contingent on these methods; even in a DSFC preparation, tumor growth results in an increasing depth of tissue through which light has to penetrate (several 100 μm). Out-of-focus light scattered by the tissue interferes with and degrades the image at the focal point, severely limiting the depth of tissue that can be examined and confounding intensity measurements and interpretation of the acquired images.[30,103] Furthermore, it is only possible to examine the vasculature in 2-D using these approaches, which introduces errors in quantitative measures of vascular morphology and function. Traditionally, the only method of examining the tumor vascular network in 3-D was through reconstruction of a 3-D image following 2-D analysis of serial immunohistochemical sections, or through vascular casting.[104]

To visualize a single optical section within the tissue, confocal laser scanning microscopy uses mirrors to scan a beam of laser light of the required fluorescence excitation wavelength point by point across the specimen. The emitted fluorescence signal is then "descanned" through a pinhole, preventing light from outside the focal plane degrading the image, thereby improving image resolution, signal-to-noise ratio, and allowing increased depth discrimination. As the microscope is focused through the specimen, a 3-D composite image is constructed.[105,106] However, the high light intensity of the beam, coupled with the need to repeatedly scan the specimen (either during the acquisition of a z-stack or time-lapse sequence), results in increased sample photobleaching and other light-induced tissue damage, which limits the usefulness of confocal fluorescence microscopy for IVM applications. Its use has been restricted primarily to postexcision analyses of fixed samples.[107,108] The ability of tumors to induce expression of VEGF in host stromal cells with fibroblast-like morphology was demonstrated using IVM confocal microscopy of murine mammary adenocarcinoma tumors (MCaIV) growing in VEGF-EGFP transgenic mice.[109] However, further analyses to determine spatial relationships was carried out using multiphoton microscopy techniques (see Sec. 8). One recent study utilized confocal reflected light microscopy in conjunction with multiphoton microscopy to develop a method of repeatedly and reproducibly locating the same region within a DSFC window.[110] Reflected light confo-

cal microscopy can be used to image microparticles, in this case latex polystyrene microspheres positioned in the DSFC preparation.

Basic confocal fluorescence microscopy can take considerable time, which makes it unsuitable for studies that require high spatial and temporal resolution, for example with a moving specimen. Spinning disk confocal microscopy uses a rotating Nipkow disk (with multiple pinholes each containing a microlens) to scan multiple beams of light across the specimen at the same time. The Nipkow disk can rotate as many as 1800 to 5000 times per minute, and a cooled CCD camera is normally used that allows the acquisition of up to approximately 1000 whole optical sections (frames or fields) per second,[111] thereby making it possible to view rapidly occurring events in real time.[68] The application of multiple lower intensity beams reduces photobleaching relative to confocal laser scanning microscopy; however, the Nipkow disks have pinholes of a fixed size and are therefore only optimized for use with one objective lens. The sensitivity and cost of the camera are other limiting factors. Nonetheless, this technique could prove invaluable in studies examining the movement of different cells and molecules during the dynamic process of tumor angiogenesis.

Another approach to real-time confocal IVM is video rate confocal laser scanning microscopy (VRCLSM), which has been applied to *in vivo* studies of kidney function.[112,113] VRCLSMs usually employ an acousto-optical deflector to scan the laser beam at high speed across the specimen. Early applications of this technique usually produced video signals which could be recorded to tape, although more recent VRCLSM systems tend to be modules that are added to conventional CLSM.

8 Multiphoton Fluorescence Microscopy

Since 1990 when its potential as a biological imaging tool was clearly established,[114] multiphoton microscopy has been growing in strength and has played a key role in many biological studies examining tumor angiogenesis.[29,38,115] Multiphoton microscopy uses short pulses (approximately 100 femtoseconds) of high intensity infrared (IR) or near-infrared (NIR) light to induce multiple photon excitation.[105,114,116] For fluorescence to occur, a fluorophore must first absorb a photon of light that has energy appropriate to induce an excited state. This usually happens with the arrival of a single photon, but can also occur if two photons with half the energy (or three with one third…etc.) are absorbed almost simultaneously. Since it is extremely unlikely that a significant number of lower energy (longer wavelength) photons will arrive almost simultaneously by chance, excitation of the fluorophore will only ever occur in the presence of an extremely high density of photons, found only when the beam of a powerful laser is at its most concentrated, right at the point of focus. The beam is scanned over the specimen as before but, unlike a confocal laser scanning microscope, no pinhole is required to exclude out-of-focus light, since there is no excitation of the fluorophore and therefore no photobleaching above and below the plane of focus.[30,105]

Multiphoton microscopy offers several advantages over confocal microscopy for live-tissue imaging. The low linear absorption of IR and NIR light by most tissue samples increases the depth penetration possible from the approximately 40 to 100 μm achievable using confocal microscopy to several hundred micrometers (absolute depth is dependent on the tissue properties, wavelengths used, and working distance of the objective lens). Further, as fluorophore excitation occurs exclusively within the focal plane, extensive photobleaching and tissue phototoxicity are avoided.[30,105,114,117,118]

Multiphoton fluorescence microscopy allows the excitation and visualization of fluorescent molecules, therefore unlabeled tissues are only visible when they exhibit autofluorescence (which is generally less in evidence than with single photon imaging techniques). To see weak fluorescence, a low autofluorescence background is desirable, but it can then be difficult to localize and understand the relationship between the fluorescently labeled and unlabeled tissues. It is often not possible or worthwhile to use transmitted light because of the depth of penetration in tissue or opacity of the specimen under examination, so reflection microscopy must be employed. In addition to conventional reflected light imaging, a process called second harmonic generation [SHG; see Fig. 3(b)] can be used to view noncentrosymmetric structures such as collagen.[118,119] SHG is the result of multiple photons interacting with structures such as collagen, and, as there is no loss, the energy of two photons is combined to emit twice the energy and thus half the wavelength.[118] Put simply, two photons are reflected as one photon with half the wavelength. Although not widely applied to IVM studies for examining tumor angiogenesis, SHG has been used in combination with multiphoton imaging of fluorescently labeled molecules to provide 3-D data on the spatial distribution of vessels and collagen in human melanoma tumors (Mu89),[119] and there is scope for its broader use.

Multiphoton microscopy is widely applicable to tumor angiogenesis studies using IVM and has been used to build on and improve existing knowledge. Multiphoton microscopy analyses of murine mammary and human colon adenocarcinoma tumors (MCaIV and LS174T, respectively) treated with a neutralizing antibody against VEGFR2 (DC101) clearly demonstrated therapy-induced normalization of the tumor vasculature.[101] This phenomenon was first documented using conventional fluorescence microscopy in hormone-dependent tumors.[120] Brown et al.[109] used multiphoton fluorescence microscopy to expand on a previous study demonstrating tumor cell driven expression of VEGF in host stromal cells,[121] and showed that these cells were located both at the tumor-host stroma boundary and also deep in the tumor tissue (200 μm), where they were often associated with tumor blood vessels. Accurate details on individual cell expression and spatial distribution relative to other cells and structures have only been made possible through the development of multiphoton microscopy techniques. The same study went on to demonstrate specific gene expression mediated tumor cell homing (Hif1$^{-/-}$ mutant cells homed to hypoxic regions) to track delivery of a therapeutic agent, characterize tumor vascular architecture in 3-D, and examine functional features such as blood flow velocity and permeability.[109]

Multiphoton microscopy is also useful for techniques requiring quantification of fluorescence intensity, since it overcomes some limitations of conventional fluorescence microscopy such as fluorescence scatter from outside the focal plane,

for example in estimation of tumor vascular permeability [see Fig. 3(c)]. Using multiphoton microscopy, the VDA, CA-4-P was found to rapidly increase vascular permeability to a 40-kD dextran in the P22 rat sarcoma tumor model,[29] and a high molecular weight isoform of VEGF (VEGF188) was found to be associated with development of tumor blood vessels with improved barrier function compared with lower molecular weight isoforms (VEGF164 and 120).[38] Further data on the possible molecular mechanisms behind tumor vascular maturity, and subsequent impact on treatment, was provided in a study using a wild-type human glioblastoma model (U87MG) and a variant stably transfected to overexpress PDGF-C.[115] Multiphoton microscopy was used to examine vascular architecture and permeability (as a measure of function). PDGF-C was found to play an important role in glioblastoma vascular maturation, with the PDGF-C overexpressing tumors demonstrating a more normalized vascular morphology concurrent with decreased vascular leakiness. Consistent with improved vascular maturity, the PDGF-C overexpressing tumors also demonstrated resistance to treatment with DC101.[115]

9 Hyperspectral Imaging

Hyperspectral imaging is a technique based on the absorbance of light across a spectrum of wavelengths by different tissues.[122] The technique may be used with either transmitted light if the specimen is thin enough or reflected light. The primary application of this technique for *in vivo* imaging of tumor vasculature is to examine metabolic data, or more specifically vascular oxygen saturation. Oxy- and deoxyhemoglobin demonstrate differences in light absorption (both visual and NIR light can be used) in proportion with the level of oxygen saturation.[122–124] Consequently, oxygen saturation within tumor vessels can be measured [see Fig. 3(d)] in real time through the use of IVM in conjunction with an appropriate optical filtering system, such as an acousto-optic or liquid crystal tunable filter, which is fitted in front of the camera.[123,125] The potential of this technique to study oxygenation in tumor blood vessels has been clearly demonstrated in a study using the 4T1 mammary carcinoma tumor model. The tumor model was engineered to express GFP under the control of a HRE, as well as to constitutively express RFP. Thus, tumor growth and the onset of hypoxia could be monitored using fluorescent IVM. Through the simultaneous application of hyperspectral imaging, filtering the absorption bandwidth within the appropriate hyperspectral range, oxygen saturation "maps" showing the spatial distribution of oxyhemoglobin were produced.[125] Using this method, the same group has recently related fluctuations in tumor microvascular oxygenation to the location of arteriovenous shunts, a common anomaly in tumor vascular networks.[8]

10 Optical Coherence Tomography

Optical coherence tomography (OCT) is a noninvasive optical imaging technique that can be used to generate high resolution 3-D images, at depth, alongside additional information on blood flow.[126–129] It shares several similarities to ultrasound imaging but is based on measuring the intensity and time delay of light, rather than sound, back-scattered by tissue. The use of a weakly focused optical beam is used to generate sectioned images over an axial range of several millimeters. Generation of the image is based on a fiber optic Michelson interferometer and low-coherence wavelength light source.[130] Briefly, light from a broad-band, single-mode source (e.g., a superluminescent diode) is sent through a beamsplitter; one beam, a reference path, is reflected from a mirror or optical delay, while the other passes down a fiber optic probe and is focused on the target specimen. Light reflected back down the reference and specimen paths is recombined, and when the distance traveled by both paths is within the coherence length of the light, interference fringes are produced. These fringes can then be analyzed to reveal changes in the intensity and back-scattered (echo) time delay produced by structures within the tissue, and a map of the tissue structure can be generated.[130] The use of light scatter to generate image contrast as opposed to fluorescence emission (e.g., confocal or multiphoton microscopy) or molecular absorption (e.g., hyperspectral microscopy) permits the use of much longer wavelengths. OCT typically operates between 800 and 1300 nm, where tissue scattering and absorption are minimized; hence, depth penetration can exceed 1 mm.

OCT is often used in conjunction with Doppler (DOCT) to examine microvascular blood flow, thereby generating high resolution images of the vascular network overlain with blood flow information.[130] OCT can provide useful information on the microstructure of the tumor vasculature without the need for fluorescent probes. Further, the application of DOCT and the generation of image analysis techniques such as speckle variance analysis[127] permits the acquisition of blood flow data that may be spatially attributed to the vascular map.

So far, OCT/DOCT-based technology has been applied primarily to normal tissues.[130] For instance, it has been used to observe photodynamic therapy (PDT)-induced vascular shutdown of normal blood vessels using IVM in the DSFC.[127] However, tumor studies are beginning to emerge. In 2008, Standish et al.[131] used interstitial DOCT, where a DOCT probe was inserted into rat prostate tumors (Mat-Ly-Lu) growing subcutaneously to quantify tumor vascular response to PDT. In 2009, Vakoc et al.[132] used a modified DOCT technique, optical frequency domain imaging (OFDI)[133,134] for IVM-based high-resolution, deep tissue imaging studies of tumor vascular networks and their response to targeted therapeutics. This extensive study examined mophological features of multiple tumor blood and lymphatic vascular networks at depths beyond 1 mm (as opposed to the approximately 400-μm depth possible using multiphoton microscopy), extracting quantitative data pertaining to the structure and extent of the vascular networks through the postimaging application of an in-house automated 3-D vascular tracing and analysis algorithm. In addition to generating anatomical data on the vascular networks, which was found to correlate well with previously extracted multiphoton data, the technique was applied to tumor-bearing mice (murine mammary adenocarcinoma, MCaIV) treated with the VEGFR2 neutralizing antibody DC101, providing data on blood and lymphatic vascular changes in response to therapy. The data obtained were, again, complementary to previously acquired data using multiphoton microscopy; however, additional data were provided through the ability to image frequently (2-h time points over a 48-h period) without the use of exogenous markers. Thus, the au-

thors were able to acquire vascular networks at depths over a wide tumor volume at multiple time points without any confounding factors such as leak or photobleaching of fluorescent dyes. The ability to generate temporal and spatial data of the lymphatic vascular network, simultaneous to acquisition of blood vessel networks, was particularly novel.[132]

Thus, there is the potential for future tumor-based IVM studies using DOCT-based technologies to examine the vascular effects of various therapeutic approaches. Further, as has already been done in normal blood vessels, it could be used in combination with other optical imaging approaches such as hyperspectral imaging to examine multiple tumor vascular parameters.[135]

11 Image Analysis

Quantifying IVM data is an on-going challenge that needs to be undertaken to fully interpret the vast amounts of imaging data that can now be acquired. In addition to expensive commercial software packages, freeware such as ImageJ are available to researchers for this purpose. Alternatively, researchers often employ programming tools such as Matlab™, Mathematica™, and the similar freeware options Scilab and Octave, to develop their own algorithms for specialized analytical purposes. A common necessity for studies of tumor microcirculation is accurate identification of the vascular networks in software, so that morphological parameters can be measured, for example, or other features of the tumor microenvironment can be spatially related to the microvasculature. Barber et al.[78] proposed a semiautomatic tracing algorithm for tumor blood vessels based on a compact Hough transform and radial maps, where plasma was fluorescently labeled with intravenously administered FITC-dextran to highlight vessels under two-photon excitation. The software requires a high degree of manual tracing, but finds vessel centers and calculates vessel diameters automatically. An adaptive irregular cylinder was used to model vessels in the automated methodology proposed by Abdul-Karim et al.,[81] again using fluorescent dextran to provide contrast in SCID mice bearing a murine mammary adenocarcinoma. An automatic seeding sequence was used to localize the cylinder model, which found the center as the maximum intensity and fitted the diameter with a median calculation. Another automated methodology to trace vessels identified by fluorescent dextran is presented in Tyrrell et al.,[82] where the spatial drop in intensity of the vessels is modeled as super-Gaussian functions. The modeling was similar to Abdul-Karim et al.,[81] but instead of a cylinder, the shape model was generalized to a super-Gaussian function of the intensity, which benefits from stronger fitting in the presence of noise. Another approach, developed for computed tomography but with clear application to IVM, is based on the intensity spatial variation found through the derivatives in the directions of rows and columns (the eigenvalues of the Hessian matrix) for the discrimination of structures that resemble vessels; the diameters are then calculated from the maximum direction of change of intensity near the vessels.[136]

Data from the different optical imaging acquisition technologies described are acquired in the same format; an intensity value i (which is dependent on the number of photons detected, which in turn depends on the presence of a certain structure or concentration of a certain substance on the sample) is assigned to each element of a 5-D matrix or a subset of it. The matrix $\mathbf{i}(x,y,z,\lambda,t)$ describes the intensity as a function of the x,y,z spatial coordinates, λ is the wavelength or frequency and time is t. The spectral decomposition can be obtained with a multispectral camera or simply with a color camera with filters for the red, green, and blue channels.

IVM is being developed in parallel with a number of other sophisticated imaging technologies such as magnetic resonance imaging (MRI) and positron emission tomography (PET). Therefore, an immediate challenge is to correlate data that are derived from an individual subject with different acquisition modalities [generating separate matrices $\mathbf{i}^*(x,y,z,t,\ldots)$] to provide a detailed and spatially resolved profile of vascular parameters, drug distributions, etc. DSFCs have been modified to be used with a MRI scanner[137] to compare parameters such as tumor area, vascular area fraction, and length of large vessels with initial extraction fraction and perfusion per unit tumor volume of the MRI contrast agent gadopentetate dimeglumine (Gd-DTPA). In Sefcik et al.,[138] IVM, microcomputed tomography, and histology were used to assess microvascular remodeling and associated bone healing *in vivo* in response to the release of the bioactive phospholipid sphingosine 1-phosphate. The potential that may be achieved by combining IVM with genome-wide "-omic" approaches is discussed in Megason and Fraser.[139] The matrix $\mathbf{i}(x,y,z,t,g)$ is presented as the description of hypothetical subcellular localization patterns for all proteins in the genome, at all developmental times and places, in 3-D within an organism.

While images from IVM can be acquired with high resolutions in a short time, other techniques may require longer times for lower resolutions; therefore it is important to consider the spatiotemporal differences of the datasets while correlating and interpreting them. Another important issue arises from the actual size of the datasets. 5-D sets can easily become too large and complex to be stored, transported, and processed with the current computational resources. A final challenge will be to feed the data extracted from IVM into the mathematical models of tumor angiogenesis that have been developed recently.[140] The assumptions and parameter settings that make up these models need to be tested with experimental data before the models can be used to test hypotheses for therapeutically targeting the tumor microcirculation.

12 Summary

It is clear that IVM approaches have played, and continue to play, a vital role in studies designed to enhance our understanding of tumor vasculature—the molecular mechanisms involved in its development, the multiple structural and functional anomalies that define, it and the changes wrought by various therapeutic approaches. However, there is still much to learn, particularly with regard to molecular control of angiogenesis and acquisition of fully quantifiable data on vascular function, with sufficient spatial and numerical accuracy to allow detection of subtle changes with therapy. To address these gaps in our knowledge, it is necessary to both fully exploit and continue to build on the multiple and fast-moving technological advances in the field of optical imaging, from image and video capture to data analysis. For instance, the full potential of the more recently developed molecular probes has

not been realized in IVM studies of tumor vasculature. The expense of modern microscope systems, such as multiphoton fluorescence, has also limited their application in this field. Nevertheless, the availability of these novel tools, combined with the availability of powerful computers for data analysis and storage, guarantees a place for IVM in future investigations of tumor microcirculation. These studies will not be confined to the preclinical arena. Deep-seated human tumors will be accessible to IVM via microendoscopy, and simultaneous application of IVM with other imaging modalities in clinical use, such as MRI and PET, provides an opportunity to maximize the advantages and overcome the disadvantages of each modality. In conclusion, we expect that IVM will continue to play a valuable role in research into tumor microcirculation and make a valuable contribution to the development of cancer treatments designed to target tumor vasculature.

References

1. J. Folkman, "Tumor angiogenesis: therapeutic implications," *N. Engl. J. Med.* **285**(21), 1182–1186 (1971).
2. J. Folkman, "Angiogenesis-dependent diseases," *Semin. Oncol.* **28**(6), 536–542 (2001).
3. J. Folkman, "Role of angiogenesis in tumor growth and metastasis," *Semin. Oncol.* **29**(6 suppl 16), 15–18 (2002).
4. P. Baluk, S. Morikawa, A. Haskell, M. Mancuso, and D. M. McDonald, "Abnormalities of basement membrane on blood vessels and endothelial sprouts in tumors," *Am. J. Pathol.* **163**(5), 1801–1815 (2003).
5. H. F. Dvorak, J. A. Nagy, and A. M. Dvorak, "Structure of solid tumors and their vasculature: implications for therapy with monoclonal antibodies," *Cancer Cells* **3**(3), 77–85 (1991).
6. H. F. Dvorak, J. A. Nagy, J. T. Dvorak, and A. M. Dvorak, "Identification and characterization of the blood vessels of solid tumors that are leaky to circulating macromolecules," *Am. J. Pathol.* **133**(1), 95–109 (1988).
7. A. Eberhard, S. Kahlert, V. Goede, B. Hemmerlein, K. H. Plate, and H. G. Augustin, "Heterogeneity of angiogenesis and blood vessel maturation in human tumors: implications for antiangiogenic tumor therapies," *Cancer Res.* **60**(5), 1388–1393 (2000).
8. B. S. Sorg, M. E. Hardee, N. Agarwal, B. J. Moeller, and M. W. Dewhirst, "Spectral imaging facilitates visualization and measurements of unstable and abnormal microvascular oxygen transport in tumors," *J. Biomed. Opt.* **13**(1), 014026 (2008).
9. D. Fukumura, H. A. Salehi, B. Witwer, R. F. Tuma, R. J. Melder, and R. K. Jain, "Tumor necrosis factor alpha-induced leukocyte adhesion in normal and tumor vessels: effect of tumor type, transplantation site, and host strain," *Cancer Res.* **55**(21), 4824–4829 (1995).
10. M. W. Dewhirst, "Concepts of oxygen transport at the microcirculatory level," *Semin. Radiat. Oncol.* **8**, 143–150 (1998).
11. L. Baxter and R. Jain, "Transport of fluid and macromolecules in tumors I. Role of interstitial pressure and convection," *Microvasc. Res.* **37**, 77–104 (1989).
12. S. J. Lunt, N. Chaudary, and R. P. Hill, "The tumor microenvironment and metastatic disease," *Clin. Exp. Metastasis* **26**(1), 19–34 (2009).
13. S. J. Lunt, A. Fyles, R. P. Hill, and M. Milosevic, "Interstitial fluid pressure in tumors: therapeutic barrier and biomarker of angiogenesis," *Future Oncol.* **4**(6), 793–802 (2008).
14. R. A. Cooper, C. M. West, D. P. Wilks, J. P. Logue, S. E. Davidson, S. A. Roberts, and R. D. Hunter, "Tumour vascularity is a significant prognostic factor for cervix carcinoma treated with radiotherapy: independence from tumour radiosensitivity," *Br. J. Cancer* **81**(2), 354–358 (1999).
15. R. A. Cooper, D. P. Wilks, J. P. Logue, S. E. Davidson, R. D. Hunter, S. A. Roberts, and C. M. West, "High tumor angiogenesis is associated with poorer survival in carcinoma of the cervix treated with radiotherapy," *Clin. Cancer Res.* **4**(11), 2795–2800 (1998).
16. G. Bognar, G. Ledniczky, K. E. Toth, P. Ondrejka, and R. Tamas, "Prognostic role of vascularisation and proliferation in rectal cancer with liver metastasis," *Hepatogastroenterol.* **56**(90), 367–371 (2009).
17. S. Bosari, A. K. Lee, R. A. DeLellis, B. D. Wiley, G. J. Heatley, and M. L. Silverman, "Microvessel quantitation and prognosis in invasive breast carcinoma," *Hum. Pathol.* **23**(7), 755–761 (1992).
18. E. L. Kaijzel, G. van der Pluijm, and C. W. Lowik, "Whole-body optical imaging in animal models to assess cancer development and progression," *Clin. Cancer Res.* **13**(12), 3490–3497 (2007).
19. R. Weissleder and M. J. Pittet, "Imaging in the era of molecular oncology," *Nature (London)* **452**(7187), 580–589 (2008).
20. R. J. Viola, J. M. Provenzale, F. Li, C. Y. Li, H. Yuan, J. Tashjian, and M. W. Dewhirst, "*In vivo* bioluminescence imaging monitoring of hypoxia-inducible factor 1alpha, a promoter that protects cells, in response to chemotherapy," *AJR, Am. J. Roentgenol.* **191**(6), 1779–1784 (2008).
21. T. P. Thomas, J. Y. Ye, Y. C. Chang, A. Kotlyar, Z. Cao, I. J. Majoros, T. B. Norris, and J. R. Baker, "Investigation of tumor cell targeting of a dendrimer nanoparticle using a double-clad optical fiber probe," *J. Biomed. Opt.* **13**(1), 014024 (2008).
22. P. Kim, M. Puoris″haag, D. Cote, C. P. Lin, and S. H. Yun, "*In vivo* confocal and multiphoton microendoscopy," *J. Biomed. Opt.* **13**(1), 010501 (2008).
23. C. Y. Li, S. Shan, Q. Huang, R. D. Braun, J. Lanzen, K. Hu, P. Lin, and M. W. Dewhirst, "Initial stages of tumor cell-induced angiogenesis: evaluation via skin window chambers in rodent models," *J. Natl. Cancer Inst.* **92**(2), 143–147 (2000).
24. S. Alexander, G. E. Koehl, M. Hirschberg, E. K. Geissler, and P. Friedl, "Dynamic imaging of cancer growth and invasion: a modified skin-fold chamber model," *Histochem. Cell Biol.* **130**(6), 1147–1154 (2008).
25. D. Fukumura, L. Xu, Y. Chen, T. Gohongi, B. Seed, and R. K. Jain, "Hypoxia and acidosis independently up-regulate vascular endothelial growth factor transcription in brain tumors *in vivo*," *Cancer Res.* **61**(16), 6020–6024 (2001).
26. M. W. Dewhirst, Y. Cao, C. Y. Li, and B. Moeller, "Exploring the role of HIF-1 in early angiogenesis and response to radiotherapy," *Radiother. Oncol.* **83**(3), 249–255 (2007).
27. C. C. Reyes-Aldasoro, S. Akerman, and G. M. Tozer, "Measuring the velocity of fluorescently labelled red blood cells with a keyhole tracking algorithm," *J. Microsc.* **229**(Pt 1), 162–173 (2008).
28. K. S. Oye, G. Gulati, B. A. Graff, J. V. Gaustad, K. G. Brurberg, and E. K. Rofstad, "A novel method for mapping the heterogeneity in blood supply to normal and malignant tissues in the mouse dorsal window chamber," *Microvasc. Res.* **75**(2), 179–187 (2008).
29. C. C. Reyes-Aldasoro, I. Wilson, V. E. Prise, P. R. Barber, M. Ameer-Beg, B. Vojnovic, V. J. Cunningham, and G. M. Tozer, "Estimation of apparent tumor vascular permeability from multiphoton fluorescence microscopic images of P22 rat sarcomas *in vivo*," *Microcirculation (Philadelphia)* **15**(1), 65–79 (2008).
30. G. M. Tozer, S. M. Ameer-Beg, J. Baker, P. R. Barber, S. A. Hill, R. J. Hodgkiss, R. Locke, V. E. Prise, I. Wilson, and B. Vojnovic, "Intravital imaging of tumour vascular networks using multi-photon fluorescence microscopy," *Adv. Drug Delivery Rev.* **57**(1), 135–152 (2005).
31. B. N. Giepmans, S. R. Adams, M. H. Ellisman, and R. Y. Tsien, "The fluorescent toolbox for assessing protein location and function," *Science* **312**(5771), 217–224 (2006).
32. N. C. Shaner, G. H. Patterson, and M. W. Davidson, "Advances in fluorescent protein technology," *J. Cell. Sci.* **120**(Pt 24), 4247–4260 (2007).
33. L. J. Nugent and R. K. Jain, "Extravascular diffusion in normal and neoplastic tissues," *Cancer Res.* **44**(1), 238–244 (1984).
34. F. Yuan, H. A. Salehi, Y. Boucher, U. S. Vasthare, R. F. Tuma, and R. K. Jain, "Vascular permeability and microcirculation of gliomas and mammary carcinomas transplanted in rat and mouse cranial windows," *Cancer Res.* **54**(17), 4564–4568 (1994).
35. P. Sharma, S. Brown, G. Walter, S. Santra, and B. Moudgil, "Nanoparticles for bioimaging," *Adv. Colloid Interface Sci.* **123–126**, 471–485 (2006).
36. J. Zhang, R. E. Campbell, A. Y. Ting, and R. Y. Tsien, "Creating new fluorescent probes for cell biology," *Nat. Rev. Mol. Cell Biol.* **3**(12), 906–918 (2002).
37. M. Andresen, A. C. Stiel, J. Folling, D. Wenzel, A. Schonle, A. Egner, C. Eggeling, S. W. Hell, and S. Jakobs, "Photoswitchable fluorescent proteins enable monochromatic multilabel imaging and dual color fluorescence nanoscopy," *Nat. Biotechnol.* **26**(9), 1035–1040 (2008).

38. G. M. Tozer, S. Akerman, N. A. Cross, P. R. Barber, M. A. Bjorndahl, O. Greco, S. Harris, S. A. Hill, D. J. Honess, C. R. Ireson, K. L. Pettyjohn, V. E. Prise, C. C. Reyes-Aldasoro, C. Ruhrberg, D. T. Shima, and C. Kanthou, "Blood vessel maturation and response to vascular-disrupting therapy in single vascular endothelial growth factor-A isoform-producing tumors," *Cancer Res.* **68**(7), 2301–2311 (2008).
39. G. R. Martin and R. K. Jain, "Fluorescence ratio imaging measurement of pH gradients: calibration and application in normal and tumor tissues," *Microvasc. Res.* **46**(2), 216–230 (1993).
40. G. Helmlinger, F. Yuan, M. Dellian, and R. K. Jain, "Interstitial pH and pO2 gradients in solid tumors *in vivo*: high-resolution measurements reveal a lack of correlation," *Nat. Med.* **3**(2), 177–182 (1997).
41. X. Michalet, F. F. Pinaud, L. A. Bentolila, J. M. Tsay, S. Doose, J. J. Li, G. Sundaresan, A. M. Wu, S. S. Gambhir, and S. Weiss, "Quantum dots for live cells, *in vivo* imaging, and diagnostics," *Science* **307**(5709), 538–544 (2005).
42. M. Stroh, J. P. Zimmer, D. G. Duda, T. S. Levchenko, K. S. Cohen, E. B. Brown, D. T. Scadden, V. P. Torchilin, M. G. Bawendi, D. Fukumura, and R. K. Jain, "Quantum dots spectrally distinguish multiple species within the tumor milieu *in vivo*," *Nat. Med.* **11**(6), 678–682 (2005).
43. F. Zhou, D. Xing, S. Wu, and W. R. Chen, "Intravital imaging of tumor apoptosis with FRET probes during tumor therapy," *Mol. Imaging Biol.* **12**(1), 63–70 (2009).
44. J. O. McIntyre and L. M. Matrisian, "Optical proteolytic beacons for *in vivo* detection of matrix metalloproteinase activity," *Methods Mol. Biol.* **539**, 155–174 (2009).
45. O. Shimomura, F. H. Johnson, and Y. Saiga, "Extraction, purification and properties of aequorin, a bioluminescent protein from the luminous hydromedusan, Aequorea," *J. Cell. Comp. Physiol.* **59**, 223–239 (1962).
46. O. Shimomura, "Discovery of green fluorescent protein (GFP) (Nobel lecture)," *Angew. Chem., Int. Ed. Engl.* **48**(31), 5590–5602 (2009).
47. J. S. Condeelis, J. Wyckoff, and J. E. Segall, "Imaging of cancer invasion and metastasis using green fluorescent protein," *Eur. J. Cancer* **36**(13 Spec. No.), 1671–1680 (2000).
48. C. Coralli, M. Cemazar, C. Kanthou, G. M. Tozer, and G. U. Dachs, "Limitations of the reporter green fluorescent protein under simulated tumor conditions," *Cancer Res.* **61**(12), 4784–4790 (2001).
49. J. Condeelis and J. E. Segall, "Intravital imaging of cell movement in tumours," *Nat. Rev. Cancer* **3**(12), 921–930 (2003).
50. N. C. Shaner, R. E. Campbell, P. A. Steinbach, B. N. Giepmans, A. E. Palmer, and R. Y. Tsien, "Improved monomeric red, orange and yellow fluorescent proteins derived from Discosoma sp. red fluorescent protein," *Nat. Biotechnol.* **22**(12), 1567–1572 (2004).
51. S. Graewe, S. Retzlaff, N. Struck, C. J. Janse, and V. T. Heussler, "Going live: a comparative analysis of the suitability of the RFP derivatives RedStar, mCherry and tdTomato for intravital and *in vitro* live imaging of plasmodium parasites," *Biotechnol. J.* **4**(6), 895–902 (2009).
52. K. A. Lukyanov, D. M. Chudakov, S. Lukyanov, and V. V. Verkhusha, "Innovation: photoactivatable fluorescent proteins," *Nat. Rev. Mol. Cell Biol.* **6**(11), 885–891 (2005).
53. R. Ando, H. Hama, M. Yamamoto-Hino, H. Mizuno, and A. Miyawaki, "An optical marker based on the UV-induced green-to-red photoconversion of a fluorescent protein," *Proc. Natl. Acad. Sci. U.S.A.* **99**(20), 12651–12656 (2002).
54. G. H. Patterson and J. Lippincott-Schwartz, "A photoactivatable GFP for selective photolabeling of proteins and cells," *Science* **297**(5588), 1873–1877 (2002).
55. R. Ando, H. Mizuno, and A. Miyawaki, "Regulated fast nucleocytoplasmic shuttling observed by reversible protein highlighting," *Science* **306**(5700), 1370–1373 (2004).
56. D. M. Chudakov, V. V. Belousov, A. G. Zaraisky, V. V. Novoselov, D. B. Staroverov, D. B. Zorov, S. Lukyanov, and K. A. Lukyanov, "Kindling fluorescent proteins for precise *in vivo* photolabeling," *Nat. Biotechnol.* **21**(2), 191–194 (2003).
57. G. E. Koehl, A. Gaumann, and E. K. Geissler, "Intravital microscopy of tumor angiogenesis and regression in the dorsal skin fold chamber: mechanistic insights and preclinical testing of therapeutic strategies," *Clin. Exp. Metastasis* **26**(4), 329–344 (2009).
58. J. Sandison, "A new method for the microscopic study of living growing tissues by the introduction of a transparent chamber in the rabbit's ear," *Anat. Rec.* **28**, 281–287 (1924).
59. G. Algire, "An adaptation of the transparent chamber technique to the mouse," *J. Natl. Cancer Inst. (1940-1978)* **4**, 1–11 (1943).
60. M. W. Dewhirst, C. Gustafson, J. F. Gross, and C. Y. Tso, "Temporal effects of 5.0 Gy radiation in healing subcutaneous microvasculature of a dorsal flap window chamber," *Radiat. Res.* **112**(3), 581–591 (1987).
61. S. Shan, B. Sorg, and M. W. Dewhirst, "A novel rodent mammary window of orthotopic breast cancer for intravital microscopy," *Microvasc. Res.* **65**(2), 109–117 (2003).
62. H. Hatakawa, N. Funakoshi, M. Onizuka, K. Yanagi, N. Ohshima, Y. Satoh, T. Yamamoto, and S. Ishikawa, "Blood flow does not correlate with the size of metastasis in our new intravital observation model of Lewis lung cancer," *Microvasc. Res.* **64**(1), 32–37 (2002).
63. N. Funakoshi, M. Onizuka, K. Yanagi, N. Ohshima, M. Tomoyasu, Y. Sato, T. Yamamoto, S. Ishikawa, and T. Mitsui, "A new model of lung metastasis for intravital studies," *Microvasc. Res.* **59**(3), 361–367 (2000).
64. Y. Tsuzuki, C. Mouta Carreira, M. Bockhorn, L. Xu, R. K. Jain, and D. Fukumura, "Pancreas microenvironment promotes VEGF expression and tumor growth: novel window models for pancreatic tumor angiogenesis and microcirculation," *Lab. Invest.* **81**(10), 1439–1451 (2001).
65. W. L. Monsky, C. Mouta Carreira, Y. Tsuzuki, T. Gohongi, D. Fukumura, and R. K. Jain, "Role of host microenvironment in angiogenesis and microvascular functions in human breast cancer xenografts: mammary fat pad versus cranial tumors," *Clin. Cancer Res.* **8**(4), 1008–1013 (2002).
66. K. Norrby, A. Jakobsson, and J. Sorbo, "Quantitative angiogenesis in spreads of intact rat mesenteric windows," *Microvasc. Res.* **39**(3), 341–348 (1990).
67. G. Szczesny, A. Veihelmann, S. Massberg, D. Nolte, and K. Messmer, "Long-term anaesthesia using inhalatory isoflurane in different strains of mice-the haemodynamic effects," *Lab Anim.* **38**(1), 64–69 (2004).
68. H. Tada, H. Higuchi, T. M. Wanatabe, and N. Ohuchi, "*In vivo* real-time tracking of single quantum dots conjugated with monoclonal anti-HER2 antibody in tumors of mice," *Cancer Res.* **67**(3), 1138–1144 (2007).
69. *Handbook of Biological Confocal Microscopy*, J. Pawley, Ed., 3rd ed., pp. 251–256, Springer, New York (2006).
70. P. Falus, M. A. Borthwick, and S. G. J. Mochrie, "Fast CCD camera for x-ray photon correlation spectroscopy and time-resolved x-ray scattering and imaging," *Rev. Sci. Instrum.* **75**(11), 4383–4400 (2004).
71. J. T. Bosiers, I. M. Peters, C. Draijer, and A. Theuwissen, "Technical challenges and recent progress in CCD imagers," *Nucl. Instrum. Methods Phys. Res. A* **565**(1), 148–156 (2006).
72. M. Bigas, E. Cabruja, J. Forest, and J. Salvi, "Review oif CMOS image sensors," *Microelectron. J.* **37**, 433–451 (2006).
73. G. Sluder and D. E. Wolf, "Digital microscopy," in *Methods in Cell Biology*, Vol. **72**, 2nd ed., Academic Press, San Diego, CA (2003).
74. G. Sluder and D. E. Wolf, *Video Microscopy*, 1st ed., p. 334, Academic Press, San Diego, CA (1998).
75. K. Asaishi, B. Endrich, A. Gotz, and K. Messmer, "Quantitative analysis of microvascular structure and function in the amelanotic melanoma A-Mel-3," *Cancer Res.* **41**(5), 1898–1904 (1981).
76. B. Endrich, M. Intaglietta, H. S. Reinhold, and J. F. Gross, "Hemodynamic characteristics in microcirculatory blood channels during early tumor growth," *Cancer Res.* **39**(1), 17–23 (1979).
77. *Angiogenesis: An Integrative Approach From Science to Medicine*, W. D. Figg and J. Folkman, Eds., p. 601, Springer Science+Business Media, LLC, Berlin (2008).
78. P. R. Barber, B. Vojnovic, S. M. Ameer-Beg, R. J. Hodgkiss, G. M. Tozer, and J. Wilson, "Semi-automated software for the three-dimensional delineation of complex vascular networks," *J. Microsc.* **211**(Pt 1), 54–62 (2003).
79. G. M. Tozer, V. E. Prise, J. Wilson, M. Cemazar, S. Shan, M. W. Dewhirst, P. R. Barber, B. Vojnovic, and D. J. Chaplin, "Mechanisms associated with tumor vascular shut-down induced by combretastatin A-4 phosphate: intravital microscopy and measurement of vascular permeability," *Cancer Res.* **61**(17), 6413–6422 (2001).
80. M. E. Hardee, Y. Cao, P. Fu, X. Jiang, Y. Zhao, Z. N. Rabbani, Z. Vujaskovic, M. W. Dewhirst, and M. O. Arcasoy, "Erythropoietin blockade inhibits the induction of tumor angiogenesis and progression," *PLoS ONE* **2**(6), e549 (2007).

81. M. A. Abdul-Karim, K. Al-Kofahi, E. B. Brown, R. K. Jain, and B. Roysam, "Automated tracing and change analysis of angiogenic vasculature from *in vivo* multiphoton confocal image time series," *Microvasc. Res.* **66**(2), 113–125 (2003).
82. J. A. Tyrrell, V. Mahadevan, R. T. Tong, E. B. Brown, R. K. Jain, and B. Roysam, "A 2-D/3-D model-based method to quantify the complexity of microvasculature imaged by *in vivo* multiphoton microscopy," *Microvasc. Res.* **70**(3), 165–178 (2005).
83. G. M. Tozer, V. E. Prise, and V. J. Cunningham, "Quantitative estimation of tissue blood flow rate," *Methods Mol. Biol.* **467**, 271–286 (2009).
84. J. C. Waters, "Accuracy and precision in quantitative fluorescence microscopy," *J. Cell Biol.* **185**(7), 1135–1148 (2009).
85. K. G. Brurberg, J. V. Gaustad, C. S. Mollatt, and E. K. Rofstad, "Temporal heterogeneity in blood supply in human tumor xenografts," *Neoplasia* **10**(7), 727–735 (2008).
86. R. K. Jain, "Delivery of novel therapeutic agents in tumors: physiological barriers and strategies," *J. Natl. Cancer Inst.* **81**(8), 570–576 (1989).
87. G. M. Tozer, C. Kanthou, and B. C. Baguley, "Disrupting tumour blood vessels," *Nat. Rev. Cancer* **5**(6), 423–435 (2005).
88. F. Yuan, M. Dellian, D. Fukumura, M. Leunig, D. A. Berk, V. P. Torchilin, and R. K. Jain, "Vascular permeability in a human tumor xenograft: molecular size dependence and cutoff size," *Cancer Res.* **55**(17), 3752–3756 (1995).
89. L. E. Gerlowski and R. K. Jain, "Microvascular permeability of normal and neoplastic tissues," *Microvasc. Res.* **31**(3), 288–305 (1986).
90. N. Z. Wu, B. Klitzman, G. Rosner, D. Needham, and M. W. Dewhirst, "Measurement of material extravasation in microvascular networks using fluorescence video-microscopy," *Microvasc. Res.* **46**(2), 231–253 (1993).
91. H. C. Lichtenbeld, F. Yuan, C. C. Michel, and R. K. Jain, "Perfusion of single tumor microvessels: application to vascular permeability measurement," *Microcirculation (Philadelphia)* **3**(4), 349–357 (1996).
92. M. R. Dreher, W. Liu, C. R. Michelich, M. W. Dewhirst, F. Yuan, and A. Chilkoti, "Tumor vascular permeability, accumulation, and penetration of macromolecular drug carriers," *J. Natl. Cancer Inst.* **98**(5), 335–344 (2006).
93. S. K. Hobbs, W. L. Monsky, F. Yuan, W. G. Roberts, L. Griffith, V. P. Torchilin, and R. K. Jain, "Regulation of transport pathways in tumor vessels: role of tumor type and microenvironment," *Proc. Natl. Acad. Sci. U.S.A.* **95**(8), 4607–4612 (1998).
94. K. Jacobson, Z. Derzko, E. S. Wu, Y. Hou, and G. Poste, "Measurement of the lateral mobility of cell surface components in single, living cells by fluorescence recovery after photobleaching," *J. Supramol Struct.* **5**(4), 565(417)–576(428), (1976).
95. V. P. Chauhan, R. M. Lanning, B. Diop-Frimpong, W. Mok, E. B. Brown, T. P. Padera, Y. Boucher, and R. K. Jain, "Multiscale measurements distinguish cellular and interstitial hindrances to diffusion *in vivo*," *Biophys. J.* **97**(1), 330–336 (2009).
96. S. R. Chary and R. K. Jain, "Direct measurement of interstitial convection and diffusion of albumin in normal and neoplastic tissues by fluorescence photobleaching," *Proc. Natl. Acad. Sci. U.S.A.* **86**(14), 5385–5389 (1989).
97. M. W. Dewhirst, E. T. Ong, R. D. Braun, B. Smith, B. Klitzman, S. M. Evans, and D. Wilson, "Quantification of longitudinal tissue pO2 gradients in window chamber tumours: impact on tumour hypoxia," *Br. J. Cancer* **79**(11–12), 1717–1722 (1999).
98. Y. Cao, C. Y. Li, B. J. Moeller, D. Yu, Y. Zhao, M. R. Dreher, S. Shan, and M. W. Dewhirst, "Observation of incipient tumor angiogenesis that is independent of hypoxia and hypoxia inducible factor-1 activation," *Cancer Res.* **65**(13), 5498–5505 (2005).
99. G. Cernaianu, S. Frank, K. Erbstosser, S. Leonhardt, M. Cross, Z. McIvor, G. Scholz, T. Dansranjavin, I. Celik, A. Tannapfel, C. Wittekind, R. B. Troebs, K. Rothe, J. Bennek, J. Hauss, and H. Witzigmann, "TNP-470 fails to block the onset of angiogenesis and early tumor establishment in an intravital minimal disease model," *Int. J. Colorectal Dis.* **21**(2), 143–154 (2006).
100. M. Czabanka, M. Vinci, F. Heppner, A. Ullrich, and P. Vajkoczy, "Effects of sunitinib on tumor hemodynamics and delivery of chemotherapy," *Inhaled Part* **124**(6), 1293–1300 (2009).
101. R. T. Tong, Y. Boucher, S. V. Kozin, F. Winkler, D. J. Hicklin, and R. K. Jain, "Vascular normalization by vascular endothelial growth factor receptor 2 blockade induces a pressure gradient across the vasculature and improves drug penetration in tumors," *Cancer Res.* **64**(11), 3731–3736 (2004).
102. K. J. Williams, B. A. Telfer, A. M. Shannon, M. Babur, I. J. Stratford, and S. R. Wedge, "Combining radiotherapy with AZD2171, a potent inhibitor of vascular endothelial growth factor signaling: pathophysiologic effects and therapeutic benefit," *Mol. Cancer Ther.* **6**(2), 599–606 (2007).
103. D. Fukumura and R. K. Jain, "Imaging angiogenesis and the microenvironment," *APMIS* **116**(7–8), 695–715 (2008).
104. D. M. McDonald and P. L. Choyke, "Imaging of angiogenesis: from microscope to clinic," *Nat. Med.* **9**(6), 713–725 (2003).
105. K. Norman, "Techniques: Intravital microscopy—a method for investigating disseminated intravascular coagulation?" *Trends Pharmacol. Sci.* **26**(6), 327–332 (2005).
106. V. Prasad, D. Semwogerere, and E. R. Weeks, "Confocal microscopy of colloids," *J. Phys. Condens. Matter* **19**(11), 113102 (2007).
107. Y. S. Chang, E. di Tomaso, D. M. McDonald, R. Jones, R. K. Jain, and L. L. Munn, "Mosaic blood vessels in tumors: frequency of cancer cells in contact with flowing blood," *Proc. Natl. Acad. Sci. U.S.A.* **97**(26), 14608–14613 (2000).
108. P. Vajkoczy, M. Farhadi, A. Gaumann, R. Heidenreich, R. Erber, A. Wunder, J. C. Tonn, M. D. Menger, and G. Breier, "Microtumor growth initiates angiogenic sprouting with simultaneous expression of VEGF, VEGF receptor-2, and angiopoietin-2," *J. Clin. Invest.* **109**(6), 777–785 (2002).
109. E. B. Brown, R. B. Campbell, Y. Tsuzuki, L. Xu, P. Carmeliet, D. Fukumura, and R. K. Jain, "*In vivo* measurement of gene expression, angiogenesis and physiological function in tumors using multiphoton laser scanning microscopy," *Nat. Med.* **7**(7), 864–868 (2001).
110. M. P. S. Dunphy, D. Entenberg, R. Toledo-Crow, and S. M. Larson, "*In vivo* microcartography and subcellular imaging of tumor angiogenesis: A novel platform for translational angiogenesis research," *Microvasc. Res.* **78**(1), 51–56 (2009).
111. A. Nakano, "Spinning-disk confocal microscopy—a cutting-edge tool for imaging of membrane traffic," *Cell Struct. Funct* **27**(5), 349–355 (2002).
112. A. Boyde, G. Capasso, and R. J. Unwin, "Conventional and confocal epi-reflection and fluorescence microscopy of the rat kidney *in vivo*," *Exp. Nephrol.* **6**(5), 398–408 (1998).
113. P. Kolman, A. Pica, N. Carvou, A. Boyde, S. Cockcroft, A. Loesch, A. Pizzey, M. Simeoni, G. Capasso, and R. J. Unwin, "Insulin uptake across the luminal membrane of the rat proximal tubule *in vivo* and *in vitro*," *Am. J. Physiol. Renal Physiol.* **296**(5), F1227–1237 (2009).
114. W. Denk, J. H. Strickler, and W. W. Webb, "Two-photon laser scanning fluorescence microscopy," *Science* **248**(4951), 73–76 (1990).
115. E. di Tomaso, N. London, D. Fuja, J. Logie, J. A. Tyrrell, W. Kamoun, L. L. Munn, and R. K. Jain, "PDGF-C induces maturation of blood vessels in a model of glioblastoma and attenuates the response to anti-VEGF treatment," *PLoS ONE* **4**(4), e5123 (2009).
116. B. R. Masters and P. T. So, "Antecedents of two-photon excitation laser scanning microscopy," *Microsc. Res. Tech.* **63**(1), 3–11 (2004).
117. W. Denk and K. Svoboda, "Photon upmanship: why multiphoton imaging is more than a gimmick," *Neuron* **18**(3), 351–357 (1997).
118. R. M. Williams, W. R. Zipfel, and W. W. Webb, "Multiphoton microscopy in biological research," *Curr. Opin. Chem. Biol.* **5**(5), 603–608 (2001).
119. E. Brown, T. McKee, E. diTomaso, A. Pluen, B. Seed, Y. Boucher, and R. K. Jain, "Dynamic imaging of collagen and its modulation in tumors *in vivo* using second-harmonic generation," *Nat. Med.* **9**(6), 796–800 (2003).
120. R. K. Jain, N. Safabakhsh, A. Sckell, Y. Chen, P. Jiang, L. Benjamin, F. Yuan, and E. Keshet, "Endothelial cell death, angiogenesis, and microvascular function after castration in an androgen-dependent tumor: role of vascular endothelial growth factor," *Proc. Natl. Acad. Sci. U.S.A.* **95**(18), 10820–10825 (1998).
121. D. Fukumura, R. Xavier, T. Sugiura, Y. Chen, E. C. Park, N. Lu, M. Selig, G. Nielsen, T. Taksir, R. K. Jain, and B. Seed, "Tumor induction of VEGF promoter activity in stromal cells," *Cell* **94**(6), 715–725 (1998).
122. R. Gillies, J. E. Freeman, L. C. Cancio, D. Brand, M. Hopmeier, and J. R. Mansfield, "Systemic effects of shock and resuscitation monitored by visible hyperspectral imaging," *Diabetes Technol. Ther.* **5**(5), 847–855 (2003).

123. R. D. Shonat, E. S. Wachman, W. Niu, A. P. Koretsky, and D. L. Farkas, "Near-simultaneous hemoglobin saturation and oxygen tension maps in mouse brain using an AOTF microscope," *Biophys. J.* **73**(3), 1223–1231 (1997).
124. S. P. Nighswander-Rempel, R. Anthony Shaw, J. R. Mansfield, M. Hewko, V. V. Kupriyanov, and H. H. Mantsch, "Regional variations in myocardial tissue oxygenation mapped by near-infrared spectroscopic imaging," *J. Mol. Cell. Cardiol.* **34**(9), 1195–1203 (2002).
125. B. S. Sorg, B. J. Moeller, O. Donovan, Y. Cao, and M. W. Dewhirst, "Hyperspectral imaging of hemoglobin saturation in tumor microvasculature and tumor hypoxia development," *J. Biomed. Opt.* **10**(4), 44004 (2005).
126. J. Fingler, D. Schwartz, C. Yang, and S. E. Fraser, "Mobility and transverse flow visualization using phase variance contrast with spectral domain optical coherence tomography," *Opt. Express* **15**(20), 12636–12653 (2007).
127. A. Mariampillai, B. A. Standish, E. H. Moriyama, M. Khurana, N. R. Munce, M. K. Leung, J. Jiang, A. Cable, B. C. Wilson, I. A. Vitkin, and V. X. Yang, "Speckle variance detection of microvasculature using swept-source optical coherence tomography," *Opt. Lett.* **33**(13), 1530–1532 (2008).
128. J. M. Schmitt, "Optical coherence tomography (OCT): a review," *IEEE J. Sel. Top. Quantum Electron.* **5**(4), 1205–1215 (1999).
129. A. F. Fercher, W. Drexler, C. K. Hitzenberger, and T. Lasser, "Optical coherence tomography—principles and applications," *Rep. Prog. Phys.* **66**(2), 239–303 (2003).
130. D. Huang, E. A. Swanson, C. P. Lin, J. S. Schuman, W. G. Stinson, W. Chang, M. R. Hee, T. Flotte, K. Gregory, C. A. Puliafito, and A. Et, "Optical coherence tomography," *Science* **254**(5035), 1178–1181 (1991).
131. B. A. Standish, K. K. Lee, X. Jin, A. Mariampillai, N. R. Munce, M. F. Wood, B. C. Wilson, I. A. Vitkin, and V. X. Yang, "Interstitial Doppler optical coherence tomography as a local tumor necrosis predictor in photodynamic therapy of prostatic carcinoma: an *in vivo* study," *Cancer Res.* **68**(23), 9987–9995 (2008).
132. B. J. Vakoc, R. M. Lanning, J. A. Tyrrell, T. P. Padera, L. A. Bartlett, T. Stylianopoulos, L. L. Munn, G. J. Tearney, D. Fukumura, R. K. Jain, and B. E. Bouma, "Three-dimensional microscopy of the tumor microenvironment *in vivo* using optical frequency domain imaging," *Nat. Med.* **15**(10), 1219–1223 (2009).
133. S. Yun, G. Tearney, J. de Boer, N. Iftimia, and B. Bouma, "High-speed optical frequency-domain imaging," *Opt. Express* **11**(22), 2953–2963 (2003).
134. S. H. Yun, G. J. Tearney, B. J. Vakoc, M. Shishkov, W. Y. Oh, A. E. Desjardins, M. J. Suter, R. C. Chan, J. A. Evans, I. K. Jang, N. S. Nishioka, J. F. de Boer, and B. E. Bouma, "Comprehensive volumetric optical microscopy *in vivo*," *Nat. Med.* **12**(12), 1429–1433 (2006).
135. M. C. Skala, A. Fontanella, H. Hendargo, M. W. Dewhirst, and J. A. Izatt, "Combined hyperspectral and spectral domain optical coherence tomography microscope for noninvasive hemodynamic imaging," *Opt. Lett.* **34**(3), 289–291 (2009).
136. K. Krissian, G. Malandain, N. Ayache, R. Vaillant, and Y. Trousset, "Model-based detection of tubular structures in 3D images," *Comput. Vis. Image Underst.* **80**(2), 130–171 (2000).
137. J. V. Gaustad, K. G. Brurberg, T. G. Simonsen, C. S. Mollatt, and E. K. Rofstad, "Tumor vascularity assessed by magnetic resonance imaging and intravital microscopy imaging," *Neoplasia* **10**(4), 354–362 (2008).
138. L. S. Sefcik, C. E. Petrie Aronin, K. A. Wieghaus, and E. A. Botchwey, "Sustained release of sphingosine 1-phosphate for therapeutic arteriogenesis and bone tissue engineering," *Biomaterials* **29**(19), 2869–2877 (2008).
139. S. G. Megason and S. E. Fraser, "Imaging in systems biology," *Cell* **130**(5), 784–795 (2007).
140. M. A. Chaplain, S. R. McDougall, and A. R. Anderson, "Mathematical modeling of tumor-induced angiogenesis," *Annu. Rev. Biomed. Eng.* **8**, 233–257 (2006).
141. M. Tomura, N. Yoshida, J. Tanaka, S. Karasawa, Y. Miwa, A. Miyawaki, and O. Kanagawa, "Monitoring cellular movement *in vivo* with photoconvertible fluorescence protein "Kaede" transgenic mice," *Proc. Natl. Acad. Sci. U.S.A.* **105**(31), 10871–10876 (2008).